Spatial Distribution of Homopolymers in Block Copolymer Microdomains As Observed by a Combined SANS and SAXS Method

Satoshi Koizumi,† Hirokazu Hasegawa, and Takeji Hashimoto*

Division of Polymer Chemistry, Graduate School of Engineering, Kyoto University, Kyoto 606-01, Japan

Received April 25, 1994; Revised Manuscript Received September 26, 1994®

ABSTRACT: The morphology and spatial segmental distribution of constituent polymers, in particular binary mixtures of polystyrene-*block*-polyisoprene (SI) and homopolystyrene, either protonated (HS) or deuterated (DS), have been studied with small angle X-ray scattering (SAXS) and neutron scattering (SANS). The pure block copolymer SI used in this study has a lamellar microdomain morphology. The molecular weights of HS and DS are similar to each other and to that of the polystyrene block (PS) in SI. The SAXS results obtained for the mixtures of SI and HS show that (i) HS is solubilized in the PS microdomains and (ii) the polyisopropene lamellae have a thickness independent of the volume fraction of HS (Φ_{HS}), but their interface undulation increases with Φ_{HS}. These two findings, in turn, imply that added HS is localized in the middle of the PS microdomains, i.e., between the PS brushes emanating from the opposing lamellar interfaces of SI. This implication was further confirmed by SANS with a deuterium labeling technique; the spatial distribution of the DS segments in the SI/DS mixtures was indicated to be localized in the middle of the PS lamellae with the penetration depth of ca. 11 nm between the DS chains and the PS brush.

I. Introduction

Self-assembled structures in the solvent-cast films of binary mixtures of polystyrene-*block*-polyisoprene (SI) and protonated homopolystyrene (HS) were studied as a function of r_s, the ratio of the molecular weights of HS and polystyrene block (PS) in SI[1-5] and as a function of Φ_{HS}, the volume fraction of HS. When $r_S \ll 1$ (a criterion for the "wet brush" regime), HS tends to be solubilized into the PS microdomain, swelling the PS chains and causing a change of microdomain morphology with a long-range order.[6,7] The spherical microdomains composed of the polyisoprene block chains (PI) are dispersed randomly in the matrix of HS and PS without a long-range order ("spherical micelles") at the limit of high Φ_{HS} ($\Phi_{HS} \to 1$).[8-11] When $r_S \gtrsim 1$ (a criterion for "dry brush"), HS tends to be segregated from SI, forming a macrophase-separated morphology (at $r_S \gg 1$),[4] or to be solubilized into the PS microdomains without significant swelling of PS (at $r_S \cong 1$)[2,4] (see Figure 1 of ref 4 for possible states of A–B/A mixtures). In the latter case, HS does not significantly affect the PI microdomains in terms of their shape and size and in terms of the molecular conformations of PI. For example, for the particular SI that gives the morphology of alternating lamellar microdomains of PS and PI, as Φ_{HS} increases in the dry brush regime of $r_S \cong 1$, the mean distance between the PI lamellae increases. As $\Phi_{HS} \to 1$, the long-range spatial order of the PI lamellae is lost, while their thicknesses remain constant and uniform, resulting in the morphologies of lamellar, cylindrical, and spherical vesicles. The vesicular morphology was analyzed by small-angle X-ray scattering and transmission electron microscopy.[4,12] At $r_S \gg 1$ (still in the regime of dry brush), SI and HS undergo macrophase separation, forming the SI domains composed of alternating lamellae in the matrix of HS.[4,13]

In this paper, we will focus on the mixture satisfying $r_S \cong 1$ and extend our analysis to the localization of HS or deuterated homopolystyrene (DS) in the PS microdomains. We are concerned with the problem of how deeply HS (or DS) penetrates into the PS brush of SI. We employed small-angle X-ray scattering (SAXS) and transmission electron microscopy (TEM), both of which can make contrast between the polystyrene microphase composed of PS and HS (or DS) and the PI microphase, to characterize the morphology and the size of the microdomain structures. Furthermore, we employed small-angle neutron scattering (SANS) with a deuterium labeling technique to investigate the spatial distribution of the homopolystyrene (DS in this case) within the microdomains composed of PS and HS or PS and DS. The combination of SANS, SAXS, and TEM technique turns out to be very useful and crucial to elucidate the self-assembly of the SI and HS (or DS) mixtures satisfying $r_S \cong 1$, as will be summarized in section V.

A work similar to our study has been reported on mixtures of polystyrene or poly(methyl methacrylate) (PMMA) homopolymers with symmetric polystyrene-*block*-poly(methyl methacrylate) diblock copolymers.[14] Spatial distribution of the homopolymers in the alternating lamellae formed in the spin-coated thin films was investigated for the homopolymers with three different molecular weights using a neutron reflectivity technique. In this case the number of lamellae was limited to <10 so that the interlamellar spacing and hence the distribution of homopolymers are expected to be influenced by the effect of the air and substrate surfaces as well as the special film preparation method and the subsequent annealing procedure. In addition to this effect, the following differences may be worth noting: (i) The amount of the homopolymers loaded in our study is much larger than that in the previous work (20–80% vs 5 and 10%),[14] causing the lamellae to undulate, as will be discussed in sections III.1 and IV.1, and hence

* Author to whom correspondence should be addressed.
† Present address: Neutron Scattering Laboratory, Department of Materials Science and Engineering, Japan Atomic Energy Research Institute, Tokaimura, Ibaraki 319-11, Japan.
® Abstract published in *Advance ACS Abstracts,* November 15, 1994.

0024-9297/94/2227-7893$04.50/0

Table 1. Sample Characteristics

code	type	M_n	M_w/M_n	W_{PS}/W_{PI}[d]
H102	SI[a]	1.0×10^5	1.16	50/50
S62	HS[b]	6.2×10^4	1.03	100/0
SD63	DS[c]	6.3×10^4	1.18	100/0

[a] Polystyrene-*block*-polyisoprene. [b] Protonated polystyrene. [c] Deuterated polystyrene. [d] Polystyrene/polyisoprene ratio by wt %/wt %.

shift to a regime which the previous neutron reflectivity study has not covered because of the experimental difficulties. (ii) The segmental interaction parameter between PS (or DS) and PI is larger than that between PMMA and PS, which may give a fundamental difference in the spatial distribution of homopolymers solubilized in space. Therefore, our study here should belong to a physical regime different from the previous study[14] and hence may be hoped to contribute to our deeper understanding of the homopolymer solubilization problem.

II. Experimental Methods

1. Sample Specimens. SI block copolymer (code H102) prepared by living anionic polymerization was supplied by Kuraray Co., Ltd. Protonated homopolystyrene (HS) coded S62 and perdeuterated homopolystyrene (DS) coded SD63 were also prepared by living anionic polymerization. The characteristics of these polymers are summarized in Table 1. It is important to note that HS and DS have almost identical degrees of polymerization, which are also comparable to that of the PS block chains in the SI copolymer. All film specimens were prepared by a solution-cast method with toluene that is a neutrally good solvent for both PS and PI block chains as well as HS and DS. The solvent was evaporated slowly over 10 days at 30 °C. Thus prepared film specimens of ca. 0.5 mm thickness were annealed in a vacuum oven at 130−150 °C for 2 h to avoid the casting effect on the self-assembled structure.

2. Electron Microscopy (TEM). The self-assembled patterns in the film specimens were examined by TEM using ultrathin sections of ca. 50 nm thickness. The sample specimens were stained with osmium tetraoxide (OsO_4) vapor before and after microtoming. The PI phases are selectively stained by OsO_4 and appear dark in the electron micrographs, while the unstained PS phases appear bright.

3. Small-Angle Neutron Scattering (SANS). The SANS measurements were performed with a 20 m small-angle neutron scattering instrument (SANS-J) at the JRR-3M research reactor of Japan Atomic Energy Research Institute (JAERI) in Tokai. The scattering data were taken with a two-dimensional Risø-type detector, averaged over a sector between −15° and 15° of the azimuthal angle (see Figure 1), and corrected for the scattering from the empty cell and the absorption by the sample. The incoherent background scattering originated mainly from the hydrogen atoms in the specimens was estimated with the scattering of the pure HS specimen and subtracted from the net scattering intensity. In this study, the sample specimens were set in the sample holder with the "edge configuration" as shown in Figure 1. The ribbon-shaped film specimens of 0.5 mm thickness, 15 mm length, and 1 mm width were stacked to the thickness of 15 mm and placed with their film normals **n** parallel to the O*z*-axis and the length direction of the ribbon-shaped films along the O*y*-axis (see Figure 1 for the optical setup). The incident beam comes to the sample position along the O*x*-axis.

4. Small-Angle X-ray Scattering (SAXS). The SAXS measurements were performed with the apparatus and the operating condition that were reported elsewhere.[6] The SAXS profiles were obtained with a one-dimensional position-sensitive proportional counter (PSPC) which was set along the O*z*-axis at the position of the 2D detector in Figure 1. The film specimens were set in the sample holder with the edge configuration as illustrated in Figure 1. The SAXS profiles were corrected for air scattering, absorption, and thermal diffuse background scattering (TDS) but were not desmeared.

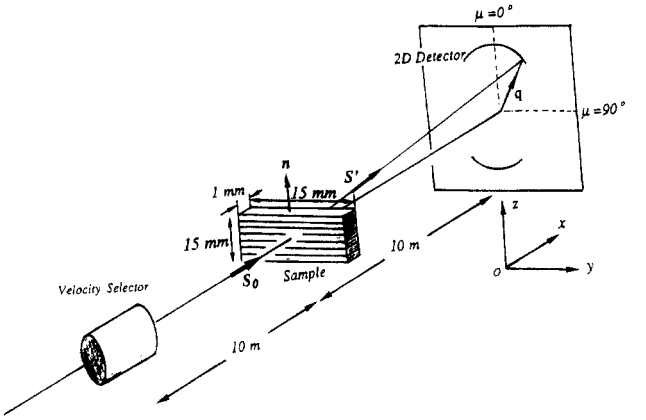

Figure 1. Optical setup for the SAXS and SANS experiments. **n** is the unit vector along the film normals, $\mathbf{S}_0$ and $\mathbf{S}'$ are the unit vectors parallel to the incident and scattered beams, respectively. **q** is the scattering vector. The Cartesian coordinate is set so that O*x* is parallel to $\mathbf{S}_0$ and the 2D detector for SANS is in O*yz* plane with the azimuthal angle $\mu = 0°$ parallel to O*z*. The PSPC for SAXS is placed along the O*z*-axis in this figure.

III. Results

1. TEM Results. Figure 2 shows electron micrographs obtained from neat SI (H102) and its mixtures with HS (S62). The blend compositions are designated by (wt % of SI)/(wt % of HS). In the micrographs, the dark regions correspond to the PI-rich domains stained by OsO_4 and the bright regions to the PS-rich domains. As shown in Figure 2a, neat SI formed alternating lamellar microdomains expected for its composition (weight fraction of PS, $W_{PS} = 0.5$). For the mixtures SI/HS, HS was completely solubilized into the PS microdomain phase, expanding the distance between the dark PI lamellae. The expansion in the interlamellar spacing causes undulation of the lamellae, resulting in a broader distribution of the spacing. The thin dark lamellae with a sharp contrast variation across their interfaces are the consequence of the edge-on view of the lamellae, i.e., the lamellar normal being oriented parallel to the ultrathin section prepared for the TEM observation. On the other hand, the thick dark (or gray) lamellae (bands) with a broad contrast variation across them are a consequence of their normals being tilted with respect to the ultrathin section (see Figure 2d). The macrophase separation between SI and HS was not observed for all of the binary mixtures studied here. The PI lamellar sheets dispersed in the matrix of PS and HS were formed, regardless of their Φ_{HS}. The preservation of the PI lamellae even at large Φ_{HS} indicates that solubilized HS does not affect the morphology of the PI microdomains. This, in turn, indicates that the penetration of HS into the brush formed by the PS block chains is not significant and the PS block chains formed the dry brush. An extensive penetration of HS into the PS brush would cause an asymmetry between the effective volume occupied by the PI chain and that of the PS chain swollen by HS. This asymmetry is expected to cause the morphological transitions with increasing Φ_{HS}.[6] The dry brush criterion will further be confirmed using the SAXS results showing that the thickness of the PI sheets is kept constant with Φ_{HS} (see Figures 9 and 10).

Figure 3 shows electron micrographs of the binary mixtures of SI/DS 80/20 and 30/70 (wt %/wt %). Here

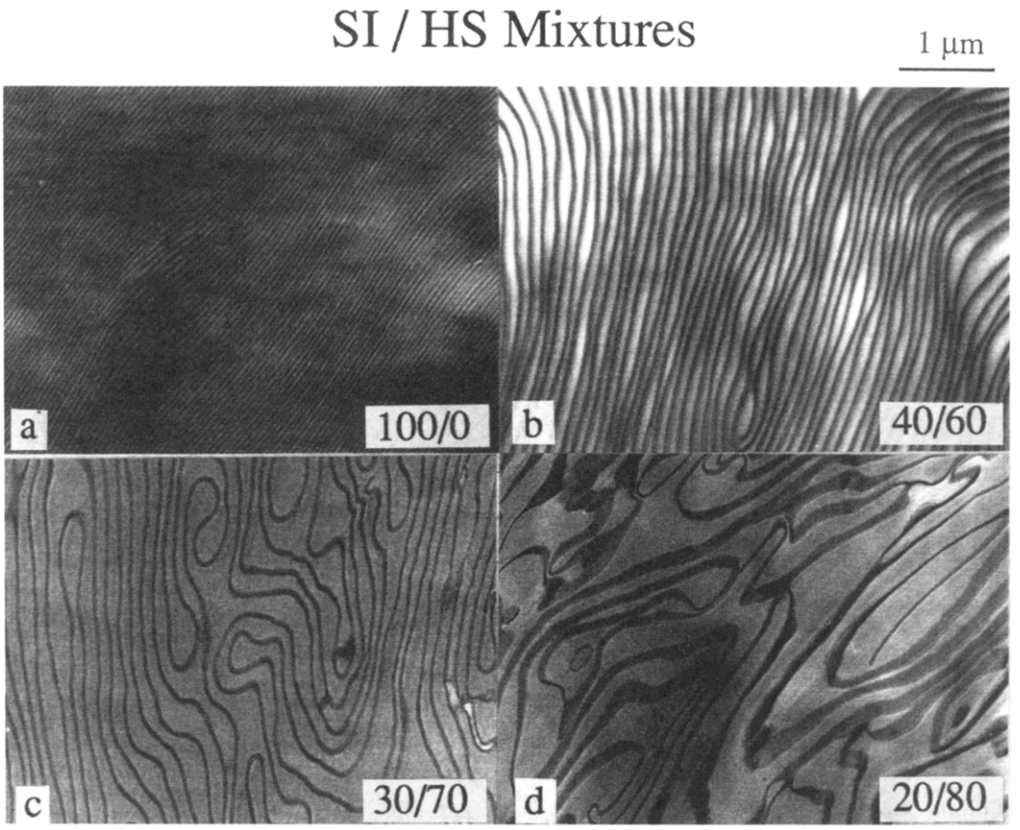

Figure 2. Electron micrographs of the binary mixtures of SI/HS with compositions of (a) 100/0, (b) 40/60, (c) 30/70, and (d) 20/80. The dark and bright regions (stained and unstained by OsO_4) correspond to the PI-rich and PS-rich phases, respectively. No morphological transition from lamellae is observed in these mixtures, but the lamellae start to undulate with increasing HS content.

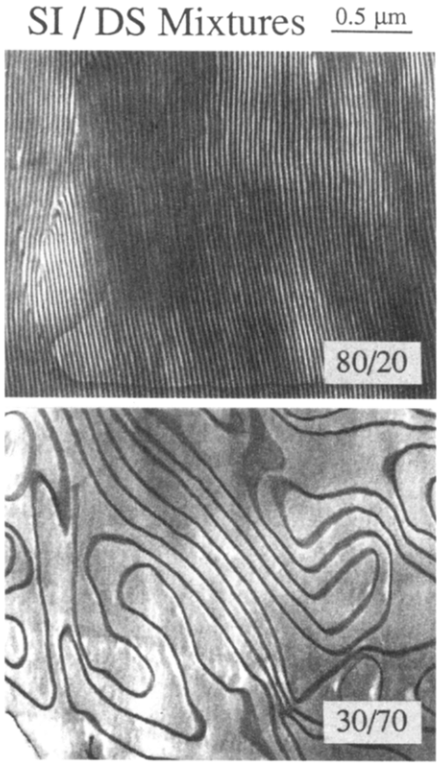

Figure 3. Electron micrographs of the binary mixtures of SI/DS with compositions of 80/20 and 30/70. The lamellae formed by SI in 30/70 are dispersed in the homopolystyrene matrix, as shown for the SI/HS mixtures in Figure 2.

we used DS, the deuterated polystyrene (SD63), instead of HS, the protonated polystyrene. We can confirm that DS was solubilized into the PS microdomain formed by the SI block copolymer, as in the case of its protonated counterpart. The dark lamellar microdomains composed of the bimolecular layers of the PI block chains are dispersed in the matrix composed of the DS chains and the PS block chains. Thus, the behavior of the SI/DS mixtures was confirmed to be identical to that of the SI/HS mixtures. It is worth noting in Figures 2 and 3 that an increase in the undulation of the PI lamellae with Φ_{HS} or Φ_{DS} (volume fraction of DS) gives rise to an increase in the absolute value of the Gaussian curvature $|K|$ of the interface;[15,16] i.e., the nature of the interface is transformed from the parabolic ($K = 0$) to the hyperbolic and/or elliptical interface ($|K| > 0$).

2. SAXS Results. All SAXS measurements have been done with the condition of edge configuration to investigate the spatial concentration fluctuations of PI against PS and HS. Figure 4 shows the relative intensity distributions of SAXS for the binary mixtures of SI/HS with various compositions, plotted double-logarithmically as a function of the magnitude of scattering vector $q = |\mathbf{q}| = (4\pi/\lambda)\sin(\theta/2)$, λ being the wavelength of the incident X-ray (Cu Kα: $\lambda = 0.154$ nm) and θ being the scattering angle. The SAXS profile of neat SI is typical of the lamellar microdomains with a long-range spatial order, showing scattering maxima at least up to the 10th order. These scattering maxima originate from interlamellar interference, and their positions are at integer multiples of the peak position for the first-order maximum (see short arrows with the integer numbers). It was observed for the mixtures having $\Phi_{HS} \leq 0.5$ that these interlamellar scattering maxima shifted toward lower q with increasing Φ_{HS} and at the same time the higher order maxima were suppressed in intensity. The shift of maxima is due to an

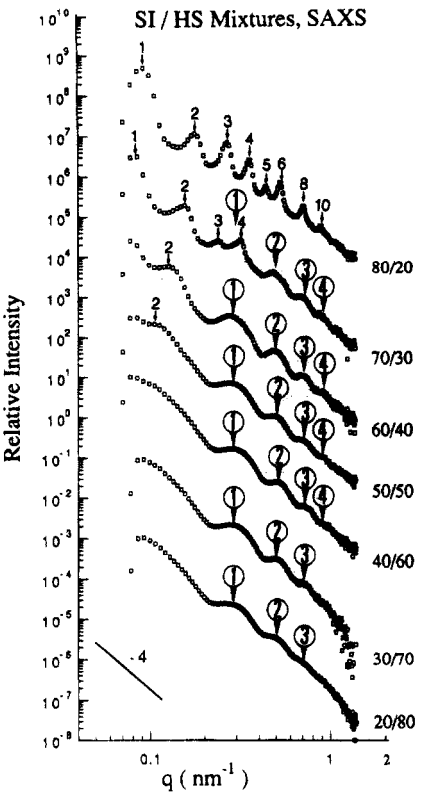

Figure 4. SAXS profiles obtained for the SI/HS (H102/S62) mixtures with compositions of 80/20, 70/30, 60/40, 50/50, 40/60, 30/70, and 20/80. The interlamellar and intralamellar scattering maxima are indicated with the integer numbers and the circled integer numbers, respectively. All of the scattering profiles are asymptotic to q^{-4} at high q in the double-logarithmic plots. The profiles are arbitrarily shifted along the intensity axis to avoid overlapping hereafter.

increase in the interlamellar spacing D, and the suppression of higher order maxima is due to broadening of the distribution of D, as will be discussed later in section IV.2.

Only the broad scattering maxima were observed for the mixtures having $\Phi_{HS} \geq 0.6$ but no sharp maxima (see thick arrows with the circled numbers 1–4). This is because of the suppression of the interlamellar scattering maxima in the higher q region. These broad maxima turned out to originate from the intraparticle interference (see section IV.2). In this case, the particles correspond to the isolated lamellae of the PI bimolecular layers. For the 70/30 mixture both the sharp interparticle interference maxima and the broad intraparticle interference maxima are simultaneously observed in low and high q regions, respectively. The existence of the higher order broad maxima, at least up to the fourth order, implies that the thickness of the PI layers is kept uniform, though the interlamellar distance is broadened. It should be noted that the positions of these broad maxima are independent of Φ_{HS} and are kept at constant q values. This result indicates that there was no morphological transition with Φ_{HS} in these mixtures and that the PI bimolecular layers maintain the constant mean thickness, inrrespective of Φ_{HS}. The only minor change observed for the mixtures with $\Phi_{HS} \geq 0.4$ is that the third- and fourth-order intralamellar interference maxima (at $q > 0.5$ nm^{-1}) become broader. This suggests that the distribution of the PI layer thickness becomes slightly broader with increasing Φ_{HS}, as will be discussed later (see section IV.2). It was found that the SAXS profiles for the SI/DS mixtures were almost identical to those for SI/HS, though not shown here.

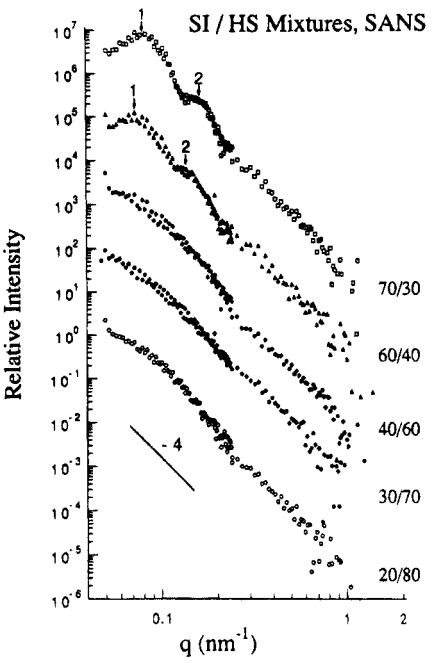

Figure 5. Sector-averaged SANS profiles obtained for the SI/HS mixtures with compositions of 70/30, 60/40, 40/60, 30/70, and 20/80. The scattering maxima originating from interlamellar interference are indicated with the integer numbers for 70/30 and 60/40. The scattering maxima originating from the intralamellar interference are hardly recognized, but all of the scattering profiles are asymptotic to q^{-4} at high q in the double-logarithmic plots.

Therefore, replacing HS by DS for the SI/HS mixtures does not affect the structure factor, which is consistent with the TEM observations (cf. Figures 2 and 3).

3. SANS Results. To confirm the instrumental q resolution of SANS-J, the binary mixtures of SI/HS studied by SAXS were also investigated with SANS-J.[17] The sample specimens were set in the sample holder with the edge configuration as shown in Figure 1. The SANS data were averaged over the sector of the azimuthal-angular range from −15° to 15° and plotted double-logarithmically in Figure 5. The q region covered by the SANS measurements is comparable with that covered by the SAXS measurements. It is noted that the PI lamellae and the matrix composed of the PS block chains and HS have a substantial difference in scattering length even without the deuterium labeling. Although the test specimens used for the two measurements are the same and the structural entities observed are also the same, the SANS scattering profiles are substantially broader than the SAXS scattering profiles. The broader SANS profiles are attributed to the greater spectral and geometrical smearing effects in SANS than in SAXS. The following points are clarified by comparing the SANS and SAXS profiles: (1) The first- and second-order peaks in the SANS profiles for 70/30 and 60/40 mixtures originate from the interparticle interference, but all of the other higher order peaks at $q \geq 0.2$ nm^{-1} observed in the SAXS profiles are smeared out. (2) All of the SANS profiles show an asymptotic behavior of q^{-n} with n being close to 4 (Porod's law[18]), which is also the case for the SAXS profiles shown in Figure 4. The interface thickness between the PS and PI phases was estimated from the asymptotic behavior of the scattering profiles in the Porod region of the SANS profiles, as will be discussed in section IV.3, and the SANS results were compared with the results estimated by SAXS, as will be discussed in sections IV.2 and IV.3.

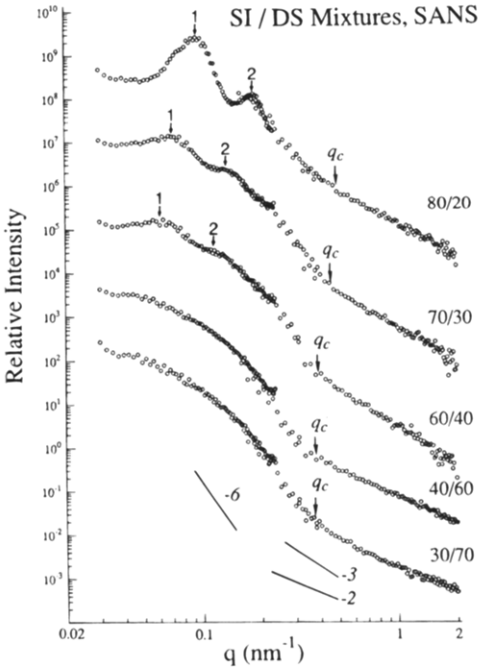

Figure 6. Sector-averaged SANS profiles obtained for the binary mixtures of SI/DS with compositions of 80/20, 70/30, 60/40, 40/60, and 30/70. The scattering maxima originating from the interlamellar interference are indicated with the integer numbers for 80/20, 70/30, and 60/40. The asymptotic behavior of the scattering profiles changes from q^{-6} at lower q than q_c to q^{-2} or q^{-3} at larger q than q_c, which is different from those observed for SI/HS by SAXS and SANS.

Figure 6 shows the SANS data for the binary mixtures of SI/DS sector-averaged over $-15° \le \mu \le 15°$. The relative scattering intensity thus obtained is plotted double-logarithmically as a function of q. The asymptotic behaviors of these profiles with q are different from those obtained from SI/HS by SAXS and SANS. Although the structural entity in the mixtures of SI/HS and that of SI/DS are identical to each other, the effective structure factor observed by SANS for the SI/DS mixtures is different from those observed by SANS for the SI/HS mixtures and by SAXS for the SI/HS and SI/DS mixtures. Here we define the critical scattering vector q_c as marked by an arrow in Figure 6. For $q < q_c$, the scattering intensity drops rapidly with the slope of about -6, while for $q > q_c$, the scattering intensity drops gradually with a slope between -2 and -3. The origin of the scattering for each region will be discussed later (see section IV.4).

IV. Analysis and Discussion

1. TEM. According to the TEM observations for SI/HS and SI/DS, the macrophase separation between SI and HS or SI and DS was not observed for all of the compositions studied in this work: HS and DS was solubilized into the PS microdomains. Furthermore, the solubilized HS (or DS) does not cause morphological changes in the PI lamellae, preserving their thin sheetlike structure composed of the bimolecular layer. The SAXS analyses as will be discussed in section IV.2 further show that the thickness of the PI lamellae is invariant with the amount of solubilized HS or DS. These results clearly indicate that the solubilized homopolymer does not significantly affect the PI lamellae. This fact, in turn, implies that the homopolymer does not significantly change the average distance a_J between the chemical junctions of SI along the SI interface and hence does not swell the PS brush of the copolymer, especially in the region near the SI interfaces. The homopolymer is expected to be localized in the center of the PS phase, implying the dry brush formation as schematically shown in Figure 7b.

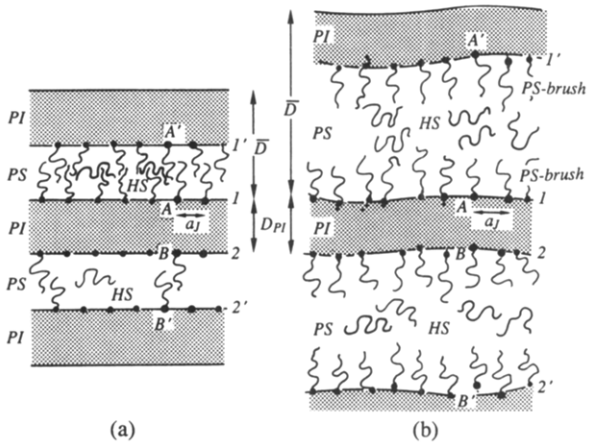

Figure 7. Schematic illustrations showing the dry brush systems formed in SI/HS mixtures with (a) a small content of HS and (b) a large content of HS, respectively. With increasing HS content, and hence increasing average interlamellar distance $\bar{D}$, the interactions between chemical junctions located on two different SI interfaces facing each other (between A and A′ or B and B′) become weaker, resulting in broadening of the distribution function for a_J, the distance between the chemical junctions along the interface as shown in (b). Most of the PS chains in the lower half of (a) are omitted.

The solubilized HS or DS expands the average spacing $\bar{D}$ between the PI lamellae, i.e., expands the PS phase. At the same time, it screens the interaction between the PS block chains which are emanating from the two SI interfaces facing each other, interfaces 1 and 1′ or 2 and 2′ in Figure 7. The screening causes the fluctuations of the amount of homopolymer HS accommodated between the PS brushes of the copolymer, which, in turn, results in the observed broadening of the distribution of the interlamellar spacing D around the mean value $\bar{D}$. However, in the case of small Φ_{HS}, as shown in Figure 7a, the interactions between the PS chains are strong, which may suppress the fluctuations of the amount of HS solubilized in the PS domains and hence the fluctuations of the interlamellar spacing D. As $\bar{D}$ increases, the PI lamellae tend to bend. In the regime where $\bar{D}$ is relatively small, the bending is collective; i.e., a stack of the lamellae is bent together, as seen in Figure 2b,c. As $\bar{D}$ further increases, bending of the PI lamellae becomes more and more independent, as seen in Figures 2d and 3b, causing the lamellae to intersect themselves or others by thermal activation to give rise to the closed loops and hence the cylindrical and spherical vesicles. The bending of the lamellae reflects the modulus or the persistence length of the lamellae. The electron micrographs clearly show that the degree of bending increases with Φ_{HS}. The bending causes an increase in absolute values of the Gaussian curvature of the interface,[15,16] giving rise to the interface as characterized by a hyperbolic or elliptic surface.

2. Paracrystal Analysis of SAXS Profiles for H102/S62. The SAXS profiles for SI/HS were analyzed using the one-dimensional paracrystal model[19,20] to elucidate the two-phase structure consisting of the PI microphase and the microphase composed of PS and HS (or DS). This model describes the one-dimensional

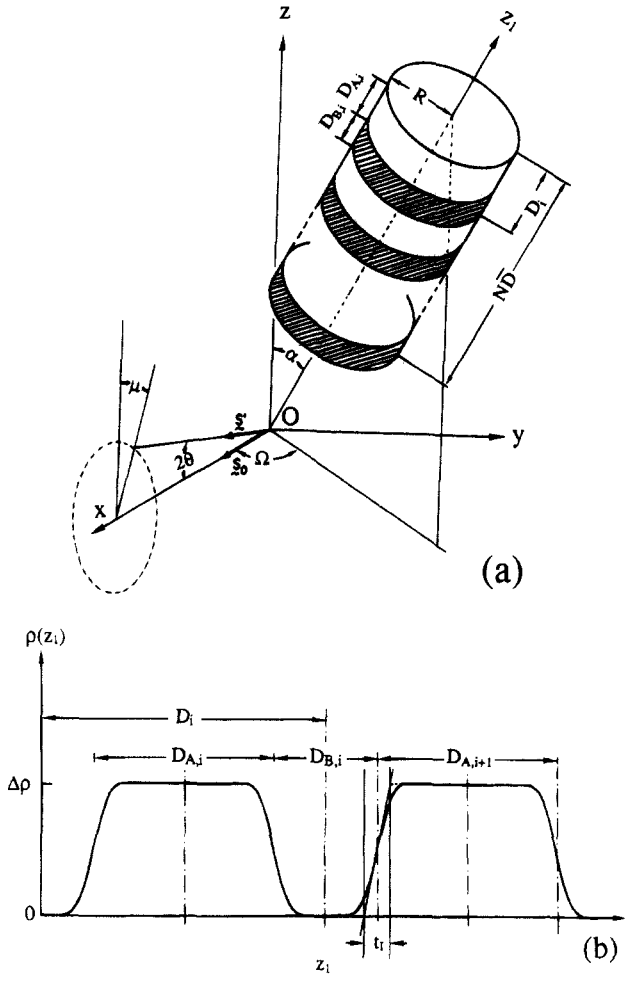

Figure 8. (a) Schematic diagram of the one-dimensional paracrystal model with respect to the laboratory-fixed Cartesian coordinate $Oxyz$. (b) Model of the spatial distribution of the relative electron density along the assembly axis z_1, $\varrho(z_1)$.

paracrystalline stack of unit disks of thickness D_i (consisting of disk A with thickness $D_{A,i}$ and disk B with thickness $D_{B,i}$, $D_i = D_{A,i} + D_{B,i}$) and radius R along the z_1-axis (parallel to the lamellar normal) as shown in Figure 8a. These stacks, which are called "grains", are arranged with a certain orientation distribution with respect to the laboratory-fixed Cartesian coordinate $Oxyz$ with the z-axis parallel to the film normal and the vertical axis of the laboratory (see Figure 1). Figure 8b shows the spatial distribution of the electron density along the z_1-axis which is characterized by interlamellar distance D_i, lamellar or disk thickness of component A $D_{A,i}$, interface thickness t_I, electron density difference $\Delta\varrho$, and number of lamellae in a stack N. In this model the interface between the A and B phases is described by a convolution product of a step function with widths $D_{A,i}$ and $D_{B,i}$, characteristic of the systems with sharp interfaces, and a Gaussian smoothing function with standard deviation[21] σ_I, characterizing the characteristic interface thickness[22] by

$$t_I = (2\pi)^{1/2}\sigma_I \quad (1)$$

The diameter of the disk $2R$ reflects the persistence length ζ of the PI bimolecular layers parallel to their interfaces, and N reflects the persistence length normal to their interfaces. As discussed in section IV.1, R and N are found to decrease with an increase in the amount of HS or DS in the mixtures. The calculation of the scattering functions for this model will be summarized in Appendix I.

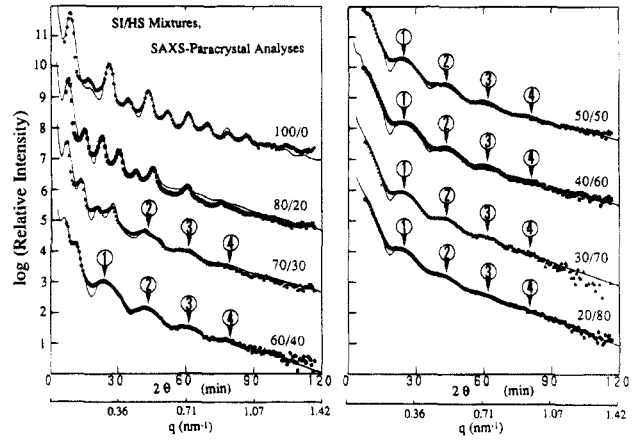

Figure 9. Best-fit scattering curves calculated with the one-dimensional paracrystal model (solid lines) to the experimental SAXS profiles of the SI/HS mixtures (data points). The scattering maxima originating from the intralamellar interference are indicated with the circled integer numbers.

The theoretical scattering profiles were smeared with the slit-height and slit-width weighting functions,[23] which were determined for the SAXS optics used in this work, to compare them with the experimental scattering profiles. The experimental scattering profiles were corrected for the thermal diffuse scattering (TDS) which was estimated by using Ruland's method[24] as described in detail in ref 4. The smeared theoretical profiles were then best-fit to the experimental profiles to obtain the characteristic parameters describing the two-phase or pseudo-two-phase structure. Figure 9 shows the best-fit theoretical profiles (solid lines) and the experimental profiles (shown by data points) for the mixtures with various volume fraction of HS. A fine agreement between the theoretical and experimental profiles were obtained as shown in Figure 9. The characteristic parameters obtained from this analysis are average interlamellar distance $\bar{D}$, average thickness of PI bimolecular layer D_{PI}, standard deviation σ_{PI} in the distribution of the thickness of PI layer, characteristic interface thickness t_I (designated hereafter $t_{I,SAXS}$) between PS and PI domains, paracrystal distortion factor g ($\equiv\sigma_D/\bar{D}$, with σ_D being a standard deviation in the distribution of the interlamellar spacing), and volume fraction of PI layer $\Phi_{PI,SAXS} \equiv D_{PI}/\bar{D}$. They are summarized in Table 2. Although there are many fitting parameters, each parameter affects the profiles substantially in different manners. Hence, the parameter assessment is fairly unique.[20,25] Here we designated the characteristic interface thickness t_I obtained by the SAXS analysis $t_{I,SAXS}$ to distinguish it from that obtained by the SANS analysis $t_{I,SANS}$. We also estimated $t_{I,SANS}$ by analyzing the SANS data in the Porod's law region as will be discussed in section IV.3. The results are also included in Table 2 and are shown to be consistent with those obtained from SAXS.

The broad maxima marked by arrows with numbers (in Figure 9) originate from the form factor of single PI layers. The magnitude of the scattering vector q_{mi} for the ith maximum and D_{PI} have the relationship

$$q_{mi}D_{PI} = 8.76, 15.14, 21.61, 27.96, 34.43, \ldots \quad (2)$$

$$(\text{for } i = 1, 2, 3, 4, 5, \ldots)$$

though these values also slightly depend on σ_{PI}.

Table 2. Characteristic Parameters Obtained for the Domain Structures of the SI/DS Mixtures from the SAXS and SANS Analyses

specimen compos	$\bar{D}^a$ (nm)	$D_{PI}{}^b$ (mm)	$\sigma_{PI}{}^c$ (nm)	$t_{I,SAXS}{}^d$ (nm)	$t_{I,SANS}{}^e$ (nm)	g^f	$\Phi_{PI}{}^g$ SAXS	$\Phi_{PI}{}^g$ volumetric
100/0	61.0 ± 1.4	32.0 ± 1.5	1.2 ± 0.04	2.0 ± 0.1		0.01	0.525	0.536
80/20	70.5 ± 2.3	30.5 ± 1.5	1.2 ± 0.04	2.0 ± 0.1		0.03	0.433	0.450
70/30	77.5 ± 1.5	30.5 ± 1.5	1.2 ± 0.04	2.0 ± 0.1	2.1 ± 0.2	0.06	0.394	0.383
60/40	95.0 ± 1.5	30.5 ± 1.0	1.2 ± 0.04	2.0 ± 0.1	2.3 ± 0.3	0.10	0.321	0.331
50/50	115.0 ± 2.0	29.9 ± 1.0	1.5 ± 0.05	2.0 ± 0.1			0.260	0.278
40/60		29.5 ± 1.2	1.5 ± 0.05	2.0 ± 0.1	2.3 ± 0.15			0.224
30/70		30.4 ± 1.2	1.5 ± 0.05	2.5 ± 0.1	2.5 ± 0.10			0.169
20/80		30.5 ± 1.2	1.7 ± 0.05	2.5 ± 0.1	2.5 ± 0.14			0.114

[a] $\bar{D}$, average interlamellar distance. [b] D_{PI}, average thickness of PI layer (lamella). [c] σ_{PI}, standard deivation of PI layer thickness. [d] $t_{I,SAXS}$, characteristic interface thickness between PS and PI phases evaluated by SAXS. [e] $t_{I,SANS}$, characteristic interface thickness between PS and PI phases evaluated by SANS. [f] g, relative standard deviation of interlamellar distance, $g = \sigma_D/\bar{D}$. [g] Φ_{PI}, volume fraction of PI layer.

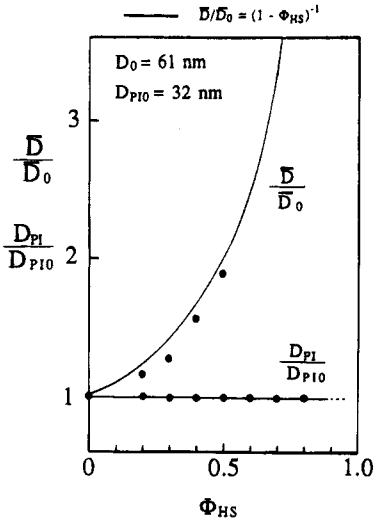

Figure 10. Average interlamellar distance $\bar{D}$ and the thickness of the PI bimolecular layers D_{PI} as a function of Φ_{HS} as evaluated by SAXS. The solid line is calculated with eq 3 predicting the change of the interlamellar distance on the assumption of no penetration of HS into the PS brush. $\bar{D}$ and D_{PI0} are $\bar{D}$ and D_{PI} for the neat copolymer, respectively.

Figure 10 shows $\bar{D}/\bar{D}_0$ and D_{PI}/D_{PI0} thus estimated by SAXS (shown by solid circles) as a function of Φ_{HS}, the volume fraction of HS in the mixtures of SI/HS where $\bar{D}_0$ and D_{PI0} are the interlamellar distance and the PI lamellar thickness for the neat SI block copolymer. If we assume that added HS is solubilized into the PS phase with the dry brush configuration, we can obtain the following formula for the change of interlamellar distance with Φ_{HS}:[4]

$$\bar{D}(\Phi_{HS}) = \bar{D}_0/(1 - \Phi_{HS}) \quad (3)$$

The experimental interlamellar distance $\bar{D}(\Phi_{HS})$ as a function of Φ_{HS} closely follows eq 3 (drawn by the solid line). On the other hand, D_{PI} is clearly independent of Φ_{HS}, as is evident from the fact that the SAXS peak positions in the form factors of single lamellae are invariant with Φ_{HS} (see Figures 4 and 9). These results indicate that the HS molecules do not deeply penetrate into the PS brushes toward the SI interface, and hence they are not significantly affecting the average distance a_J between the chemical junctions of SI along the SI interface (or the interfacial area per single copolymer chain $a_J{}^2$) (see Figure 7). Thus, it is proposed that the HS or DS molecules tend to be localized in the middle of the PS microdomains, sandwiched between the PS corona chains (or brushes) which are emanating from the interfaces facing each other (see Figure 16a). The remaining crucial question is how shallow or deep the penetration of HS or DS into the PS corona phase is. This question will be addressed in section IV.5. The volume fraction Φ_{PI} can be directly estimated from the SAXS profiles, and the results are consistent with those estimated from the volumetric consideration based on the complete segregation of PS and PI and the complete solubilization of HS into the PS microdomains (Table 2).

It was observed in Figures 4 and 9 that the higher order scattering maxima due to the interlamellar interference were not only shifted toward smaller q but also suppressed in their intensity with increasing Φ_{HS}. This suppression would result from an increase in the paracrystalline distortion factor g with Φ_{HS} (see Table 2), as a consequence of the selective solubilization of HS into the PS lamellar microdomains without undergoing the macrophase separation. This change in g or σ_D is also consistent with the TEM observation.

It is important to note that σ_{PI} as well as σ_D increases with Φ_{HS}. The increase of σ_{PI}, i.e., the increase in the polydispersity of the PI lamellar thickness with Φ_{HS}, may be closely related to the increase in $\bar{D}$. As Φ_{HS} increases, the neighboring PI lamellae become increasingly farther apart from each other, as schematized in Figure 7. Interactions between the junctions in the interface 1 and those in interface 1′ (like AA′ interaction) or between those in interface 2 and interface 2′ (like BB′ interaction) are also screened by HS (see Figure 7b). This screening may result in an increase in the fluctuations of the distance a_J and hence of D_{PI}. On the other hand, in the case of small Φ_{HS}, chemical junction A (or B) in interface 1 (or 2) is surrounded by and interacts with many junctions in the same interface or those in interface 1′ such as junction A′ (those in interface 2′ such as junction B′) and those in interface 2 such as junction B (those in interface 1 such as junction A) (see Figure 7a). These interactions would suppress the fluctuations of a_J and hence of D_{PI}. Such interactions between the junctions as described above may be important also to an interpretation on the change of the interface thickness $t_{I,SAXS}$ and $t_{I,SANS}$ with Φ_{HS}.

The increase in σ_{PI} may be partially related to the increase in the degree of bending or undulation of the PI layers with increasing Φ_{HS}, because the bending causes conformational changes of the block copolymer chains. The conformational change would cause the change in the nearest-neighbor distance of the chemical junctions of the copolymer chains along the interface, and hence it causes a change in the PI lamellar thickness; i.e., the thickness at the curved portions of the layers may be different from that at the flat portions. In this sence σ_{PI} is expected to depend on the distribution of the curvature of the layers and hence its bending modulus or persistence length ζ of the sheet.

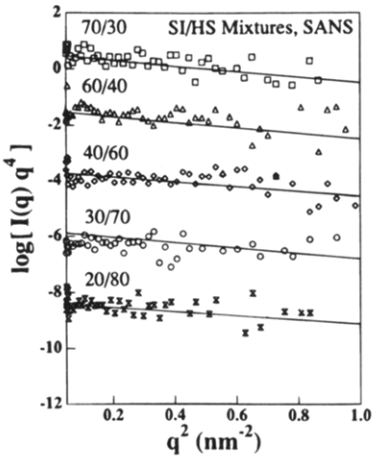

Figure 11. Porod's plots of the sector-averaged SANS profiles for the SI/HS mixtures shown in Figure 5.

3. SANS Analysis on SI/HS. The variation of the scattering length across the interface between the phase composed of PS and HS and that composed of PI can be described by a convolution product of a step function and a Gaussian smoothing function with standard deviation σ_I as denoted in section IV.2.[21] In the reciprocal space, the effect of the interface appears in the Porod region: $I(q)$ is generally steeper than that predicted from the q dependence of the scattering function by Porod's law with a sharp interface:[4] $I(q)$ in the Porod region can be given by

$$I(q) \sim q^{-4} \exp(-\sigma_I^2 q^2) \tag{4}$$

The standard deviation σ_I of the Gaussian smoothing function is related to the characteristic interface thickness t_I as defined by eq 1. Figure 11 shows the Porod plots of the scattering profiles for the SI/HS mixtures obtained by SANS. Logarithm of $I(q)q^4$ is plotted as a function of q^2, and the slopes in the figure give the characteristic interface thickness $t_{I,SANS}$ between the PS phase and the PI phase. The estimated values of the interface thickness $t_{I,SANS}$ are summarized in Table 2 and are found to be consistent with $t_{I,SAXS}$ estimated by SAXS, although these two methods are quite different.

It is important to note that the characteristic interface thickness t_I ($t_{I,SAXS}$ or $t_{I,SANS}$) increases with increasing Φ_{HS}. The same interpretation as that for the increase in σ_{PI} with Φ_{HS} may be applied to explain the above phenomenon: the screening of the interactions between the junctions in interface 1 and those in interface 1′ or between those in interface 2 and those in interface 2′ by the intervening HS (as shown in Figure 7b) may increase the positional fluctuations of the junctions normal to the interface and hence increase t_I. It should be noted that our SAXS and SANS analyses of the interface thickness t_I should be *free from the effects of the bending* of the lamellae for the following reason: the q range used in our analyses is $q \geq 0.30$ nm^{-1}, and hence the length scale L of our interest here is $L \leq (2\pi/0.3)$ nm $< D_{PI}$, smaller than the lamellar thickness. As shown clearly in Figures 2 and 3, the PI lamella interfaces are flat in this length scale L, so that we should be able to detect the true effect of the interface thickness on the scattering, free from the effect of the bending.

4. Decomposition of SANS Profiles into Domain Scattering and Scattering from Thermal Concentration Fluctuations. Using all pieces of the information obtained on the phase structure with TEM and SAXS, we now attack the problem of the spatial distribution of DS and HS in the polystyrene microdomains. Figure 12 shows a two-dimensional SANS pattern for SI/DS with 30/70 composition taken with the edge configuration shown in Figure 1. The film normal **n** is parallel to the z-axis, i.e., the horizontal direction of the pattern. The center part of the pattern around the beam stopper is highlighted at the left bottom corner of the figure. The scales indicate magnitude of scattering vector q. It should be noted that the central part of the scattering pattern at $q < q_c \cong 0.35$ nm^{-1} is directionally dependent with the highest intensity along **n**, while the outer part of the pattern at $q > q_c$ is isotopic.

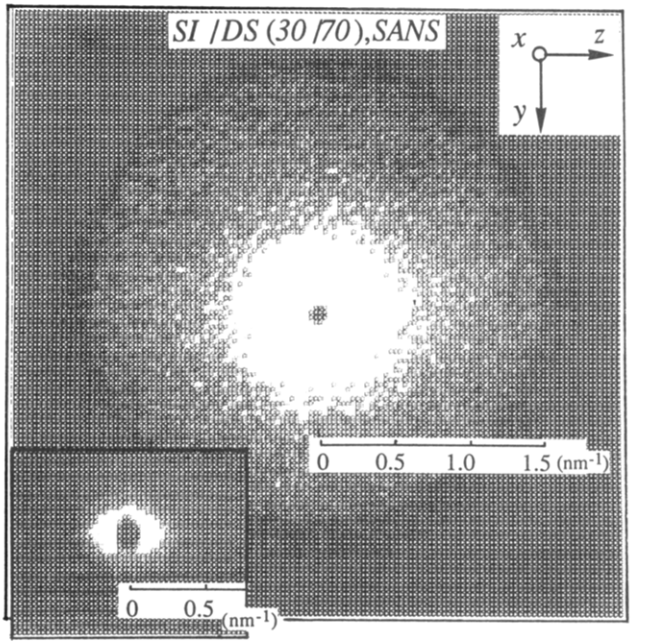

Figure 12. Two-dimensional SANS pattern obtained from the SI/DS mixture with 30/70 composition. The central part of the pattern is highlighted at the bottom left corner of the figure. The scales show the magnitude of scattering vector **q**. The central part of the scattering pattern at $q < q_c \cong 0.35$ nm^{-1} is anisotropic, exhibiting strong scattering along the z-axis, parallel to film normals **n**, while the outer part of the pattern at $q > q_c$ is isotropic.

The central part of the scattering pattern is believed to originate from the two-phase structure associated with the lamellar microdomains which are highly oriented with their interfaces perpendicular to **n**. The preferential orientation of the lamellar appears to be preserved up to high Φ_{HS}, although the degree of orientation tends to be lowered by the bending (undulation) of the lamellae. We hereafter designate this scattering from the phase structure $I_d(q)$ for the sake of convenience. On the other hand, the scattering at $q > q_c$, designated hereafter $I_t(q)$, is believed to originate from the thermal concentration fluctuations of DS and PS in the polystyrene microdomains. In the strong segregation limit, added DS is selectively solubilized into the PS microdomains but not into the PI microdomains. This solubilization induces the penetration of DS into the brush formed by the PS block chains to some extent, giving rise to the thermal concentration fluctuations of PS and DS. These fluctuations cause $I_t(q)$, because of the strong contrast between hydrogen and deuterium. The fact that $I_t(q)$ does not depend on azimuthal angle μ indicates that local concentration fluctuations of PS and DS segments in the polystyrene phase are essentially isotropic.

Therefore, total elastic scattering intensity by SANS, $I_{total}(q)$, from our system may be described by the following formula:[26]

$$I_{total}(q) = I_d(q) + I_t(q) \quad (5)$$

In the context of the mean-field random phase approximation (RPA),[27] $I_t(q)$ may be given by

$$I_t(q) \sim 1/[\phi_{PS}g(q,R_{gPS})] + 1/[\phi_{DS}g(q,R_{gDS})] - 2\chi \quad (6)$$

$$g(q,R_{gi}) = 2N_i/(qR_{gi})^4\{(qR_{gi})^2 + \exp[-(qR_{gi})^2] - 1\} \quad (7)$$

with $R_{gi} = a(N_i/6)^{1/2}$, where $g(q,R_{gi})$ is the Debye function, χ is Flory's segmental interaction parameter between PS and DS which is negligibly small ($\chi \cong 0$), R_{gi} is the radius of gyration of the ith polymer (either PS or DS), ϕ_i is the volume fraction of the ith polymer within the polystyrene microdomain, and a is the statistical segment length. Since the polymerization indices for PS and DS are almost equal to each other ($N \cong N_1 \cong N_2$), eq 4 can be simplified as

$$I_t(q) \sim \Phi_{PS}(1 - \Phi_{PS})g(q,R_g) \quad (8)$$

Equation 8 has the asymptotic behavior of q^{-2} at large q satisfying $qR_g \gg 1$, which can be observed in the high q region of the experimental SANS profiles (Figure 6). To obtain the domain scattering $I_d(q)$, $I_t(q)$ was subtracted from $I_{total}(q)$. For this purpose, $I_t(q)$ was first estimated by fitting eq 8 with the experimental SANS profiles in the high q region where the slope -2 can be observed in the double-logarithmic plots. The radius of gyration R_g used for the curve fitting was 7 nm, which was calculated from the molecular weight of the PS block of SI or that of homopolystyrene DS. The typical results of $I_t(q)$ estimated by the curve fitting are shown in Figure 13 for SI/DS with 80/20 and 30/70 compositions (broken lines). The sector-averaged net scattering profiles $I_{total}(q)$ are shown by open circles, and the scattering profiles from the phase structure $I_d(q)[=I_{total}(q) - I_t(q)]$ by solid squares or diamonds.

The above analysis shows that the net scattering profile $I_{total}(q)$ is well fitted with $I_t(q)$ given by eq 8 at a high q limit ($q \geq 1$ nm^{-1} for the 80/20 mixture and $q \geq 0.5$ nm^{-1} for the 30/70 mixture). The difference of the limiting value of q (1 vs 0.5 nm^{-1}) with the homopolymer composition may reflect the difference of the intensity level of $I_t(q)$ and hence Φ_{PS} (if the penetration depth t_P of DS and PS does not significantly change with Φ_{PS}). It should be noted, however, that the value R_g of the homopolymer DS or that of the block chain PS in the microdomains composed of PS and DS is not necessarily identical to that of the DS or PS in its own environment. Moreover, an effective R_g to be used in eq 8 in our particular problem is not necessarily 7 nm, because the penetration depth (see Figure 16) t_P is not very large compared with R_g (but rather $t_P \cong R_g$, as will be found in the next section), and hence significant composition gradients occur over a size scale of a single chain. In this sense R_g may be regarded as an adjustable parameter. An error in the subtraction of $I_t(q)$ causes an error for further analyses of $I_d(q)$.

The domain scattering $I_d(q)$ for SI/DS with 80/20 and 30/70 compositions has the asymptotic behavior of q^{-4} and q^{-6} at $q > q_c$, respectively. This difference in the asymptotic behavior of $I_d(q)$ will be fully discussed in section IV.5. Figure 14 shows thus obtained SANS domain scattering profiles $I_d(q)$ for the SI/DS mixtures.

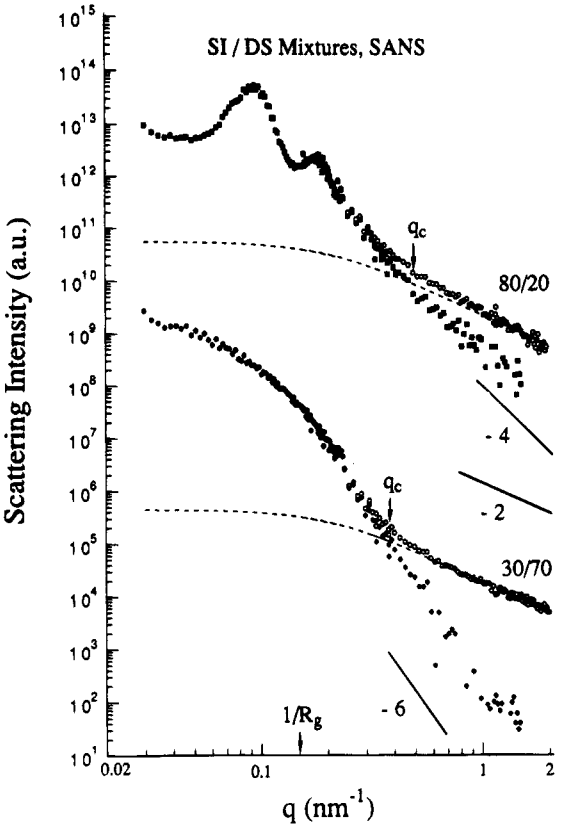

Figure 13. Examples of the estimation of the scattering caused by the thermal concentration fluctuations $I_t(q)$ for SI/DS with 80/20 and 30/70 compositions. The profiles shown by open circles, solid squares or diamonds, and broken lines denote, respectively, the sector-averaged net scattering profiles $I_{total}(q)$, the scattering profiles from the two-phase structure $I_d(q)$ [$= I_{total}(q) - I_t(q)$] and the scattering profiles due to the thermal concentration fluctuations $I_t(q)$.

It can be seen that the asymptotic behavior of $I_d(q)$ at high q changes from q^{-4} to q^{-6} as DS content increases.

5. Combined SANS and SAXS Analysis on SI/DS: Analysis of Domain Scattering. It is interesting to highlight the difference among the domain scatterings $I_d(q)$ obtained by SAXS and SANS in the same plot. Figure 15 shows three kinds of experimental scattering profiles for the mixtures with 30/70 composition: curve a, the SANS $I_d(q)$ profile for SI/DS, and curves b and c, the SANS and SAXS $I_d(q)$ profiles for SI/HS, respectively. It should be noted again that the SAXS and SANS profiles of SI/HS have the asymptotic behavior of q^{-4}, while the SANS profile of SI/DS has that of q^{-6}. According to TEM observations (Figures 2 and 3), the bimolecular layers of the block copolymers are dispersed in the matrix of HS or DS, as schematically shown in Figure 16a. In addition to the interlamellar distance $\bar{D}(\Phi_{HS})$ (or $\bar{D}(\Phi_{DS})$), there are two kinds of thickness characterizing the system: (i) the thickness of the bimolecular layers of the block copolymers as a whole D_1 and (ii) the thickness of the PI bimolecular layers D_2 as shown in Figure 16c. In the dry brush regime, D_1 should be equal to the interdomain distance D_0 (=61 nm) of pure SI, while D_2 is equal to D_{PI} (=32 nm), both of which are determined by SAXS. Two scattering structure factors calculated for the single lamellar microdomains having thicknesses of 61 and 32 nm and sharp interfaces between the two phases are also plotted in Figure 15 (curves d and e, respectively). It is confirmed that the asymptotic behavior of the SANS or SAXS profile for SI/HS is essentially identical to that for curve d or e and hence is represented by the pseudo-

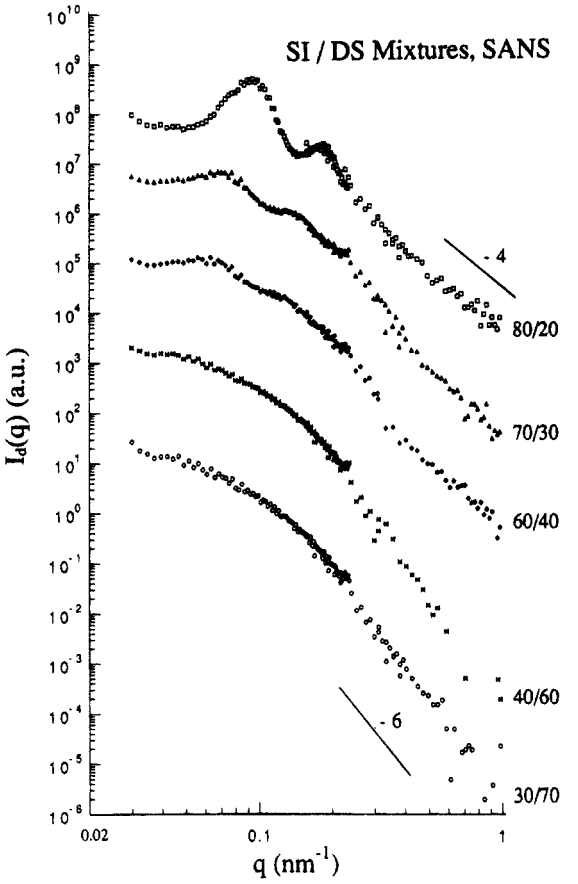

Figure 14. SANS domain scattering profiles $I_d(q)$ for the SI/DS mixtures obtained by subtracting $I_t(q)$ from $I_{total}(q)$. As DS content increases, the asymptotic behavior of $I_d(q)$ at high q changes from q^{-4} to q^{-6}.

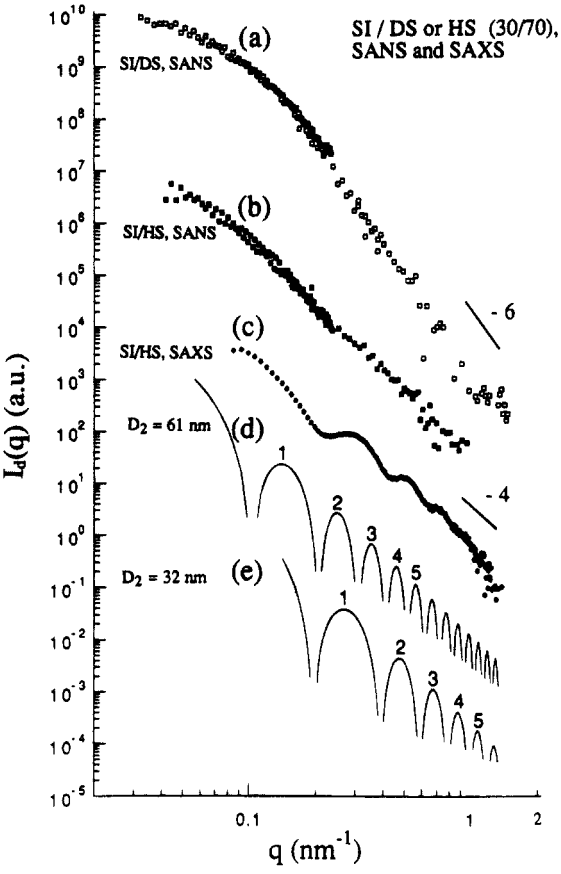

Figure 15. Comparison of scattering profiles for SI/HS and SI/DS with 30/70 composition. The scattering profiles are obtained, respectively, for (a) SI/DS by SANS, (b) SI/HS by SANS, and (c) SI/HS by SAXS. The solid lines are the calculated curves for the lamellar form factors having sharp interfaces with the thicknesses of (d) D_2 = 62 nm and (e) D_2 = 31 nm, respectively.

two-phase structure with the thin characteristic interface thickness t_I ($t_{I,SAXS}$ and $t_{I,SANS}$ in Table 2). It is obvious that the asymptotic behavior of the SANS profile for the domain structure in the SI/DS mixture (curve a) is very different from that in curve b or c, indicating that the behavior cannot be explained with the same domain structure as that for curves b and c.

To describe the SANS profile for the phase structure of the SI/DS mixture, we must consider the three-phase-lamella model which is characterized by the two kinds of layer thicknesses, D_1 and D_2, shown in Figure 16. Parts a–c, respectively, show schematically the spatial distribution of the constitutent polymers (DS, PS, and PI), that of the segmental density $\varrho_K(r)$ of the Kth polymer (K being PS, DS, or PI), and that of the neutron scattering length $B_{net}(r)$ normal to the lamellar interface for the mixtures having high DS content Φ_{DS}. On the other hand, parts d and e are $\varrho_K(r)$ and $B_{net}(r)$ for the mixtures having low Φ_{DS}, respectively. In the mixtures having high Φ_{DS}, the lamellar vesicles (the bimolecular layers) formed by SI are isolated in the matrix of DS. The interfaces between the PI and PS domains and between the PS and DS domains have finite characteristic interface thicknesses t_I and t_P, respectively. t_I can be determined by the SAXS analysis (section IV.2) and by the SANS analysis (section IV.3). The spatial variation of the scattering length for such a system may be described by a convolution product of a step function with two length scales D_1 and D_2, characterizing the systems with sharp interfaces, and two Gaussian smoothing functions with standard deviations σ_I and σ_P, characterizing the characteristic interface widths t_I and t_P (see Figure 16b,c). The former is given by eq 1 and the latter by

$$t_P = (2\pi)^{1/2}\sigma_P \tag{9}$$

In the asymptotic region of our interest, the interdomain interference function approaches unity. Hence we focus on the structure factor from the single domain with the characteristic sizes D_1, D_2, t_P, and t_I and with the characteristic contrasts ΔB_1 and ΔB_2, as shown in Figure 16c,e. ΔB_1 and ΔB_2 are the differences in scattering length between the DS-rich phase and the PS brush in the PS phase and between PS and PI, respectively. The scattering amplitude for this model with **q** vector in the direction normal to the interface, $f(q)$, is given as

$$f(q) \sim \Delta B_1 D_1[\sin(D_1q/2)/(D_1q/2)]\exp(-\sigma_P^2q^2/2) + \Delta B_2 D_2[\sin(D_2q/2)/(D_2q/2)]\exp(-\sigma_I^2q^2/2) \tag{10}$$

The scattering intensity for partially oriented or randomly oriented lamellar systems should be described as

$$I_d(q) \sim q^{-2}f(q)^2 \tag{11}$$

where the additional factor q^{-2} is the Lorentz factor discussed earlier for the lamellar systems having an orientation distribution in 3D space and their lateral dimensions much greater than their thicknesses, D_1 and

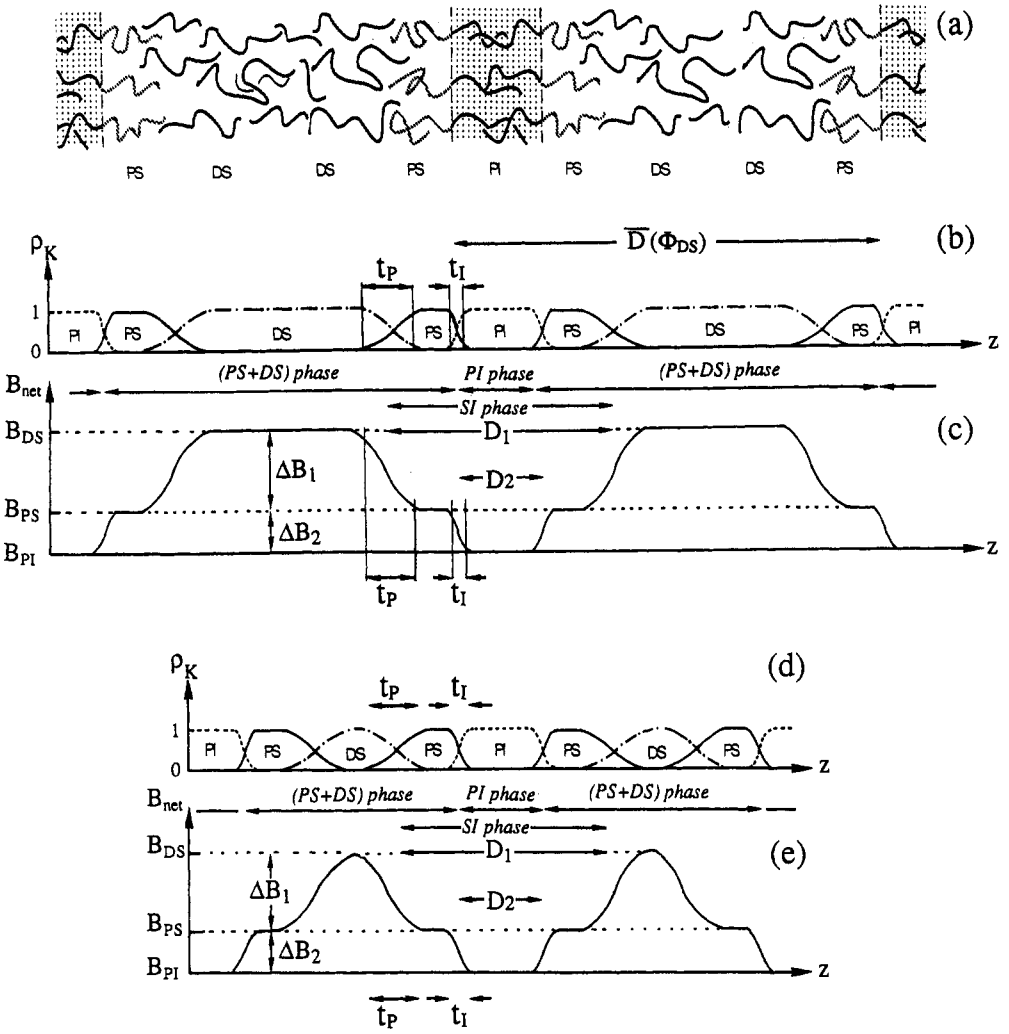

Figure 16. Schematic diagrams showing (a) the spatial distributions of DS in the SI lamellae, (b) the density profile of DS and SI, and (c) the scattering lengths along the Oz_1-axis normal to the lamellar interface. (a)–(c) show those for the mixtures with a large content of DS in which the PS brushes do not overlap each other, while (d) and (e) show those for the mixtures with a small content of DS for which the PS brushes start to overlap each other.

D_2.[20] Equation 11 has an asymptotic form given by

$$I_d(q) \sim q^{-4}[\Delta B_1 \exp(-\sigma_P^2 q^2/2) + \Delta B_2 \exp(-\sigma_I^2 q^2/2)]^2 \quad (12)$$

ΔB_1 is simply given by $\Delta B_1 = B_{DS} - B_{PS}$ when the mixture possesses such a high Φ_{DS} that the PS brushes emanating from the two interfaces do not overlap each other as shown in parts a–c or just start to overlap as shown in parts d and e in Figure 16. If Φ_{DS} is further reduced and the PS brushes overlap each other, ΔB_1 depends on the exact spatial distribution of DS, $\varrho_{DS}(z)$, and is given by $\Delta B_1 = \mathrm{Max}[\Delta B_1(z)]$, where $\Delta B_1(z) = B_{net}(z) - B_{PS}$ and $B_{net}(z) = B_{PS}[1 - \varrho_{DS}(z)] + B_{DS}\varrho_{DS}(z)$. In this case ΔB_1 is used as an adjustable parameter in our analysis. However, this is not the case of our primary interest in this work and is beyond the scope of our present paper. The lowest limit of Φ_{DS} above which our approach based upon eq 12 and the model shown in Figure 16 are applicable is roughly estimated to be 0.16 as shown in Appendix II.

For example, for the mixtures having Φ_{HS} (or Φ_{DS}) equal to 0.4, the repeat distance of the lamellae $\bar{D}$ is expected to be $\bar{D} \geq 100$ nm according to eq 3. This implies that the interlamellar interference becomes important in the q region satisfying $q \cong 2\pi/\bar{D} \leq 0.06$ nm^{-1}. However, at $q > 0.1$, the interlamellar interference function approaches unity as seen from Figure 14, and hence it is reasonable to assume that $I_d(q)$ for the system can be represented by the domain scattering given in eq 12. The following analysis will focus on the analysis of the domain scattering based on eq 12 in the q region satisfying $0.1 < q < 2.0$ nm^{-1}.

In eq 12, ΔB_1 and ΔB_2 are known in the literature, σ_I (or $t_I \equiv t_{I,SAXS}$ or $t_{I,SANS}$) was separately determined by the SAXS or SANS analysis (sections IV.2 and IV.3). The only unknown parameter is σ_P (or t_P), which is related to the penetration depth between DS and the PS brush. To determine the parameter σ_P, the experimental scattering profiles $I_d(q)$ were best-fit to the theoretical profiles obtained from eq 12. The best fits for the mixtures having the compositions from 60/40 to 30/70 were obtained under the following requirements: (i) ΔB_1 is equal to $B_{DS} - B_{PS}$; (ii) σ_I is estimated by SAXS (Table 2). Figure 17 shows the best-fit curves of eq 12 to the SANS profiles for the mixtures with the compositions from 60/40 to 30/70. The SANS analysis for the mixtures 80/20 and 70/30, the curve-fitting of which was different from the others, will be discussed later. The asymptotic behavior of the SANS profiles was well reproduced by that given by eq 12 (solid lines). Thus, the characteristic interface thickness between DS and the PS brush t_P was determined as ca. 11 nm,

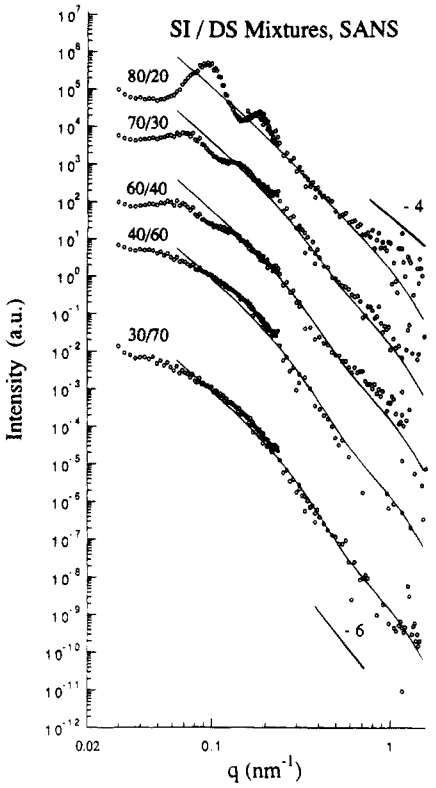

Figure 17. Best-fit scattering curves (solid lines) calculated by eq 12 to the domain scattering $I_d(q)$ obtained by SANS.

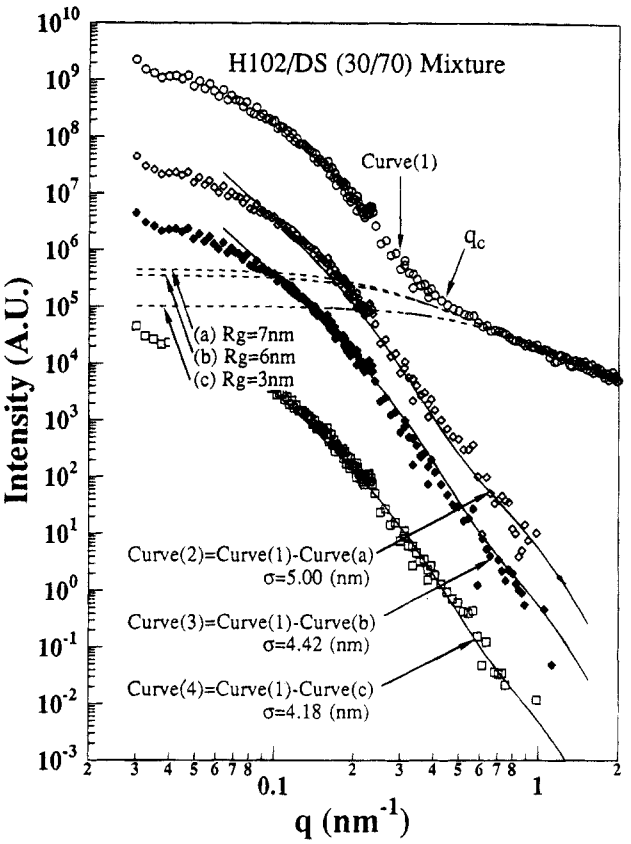

Figure 18. Dependence of the best-fit $I_d(q)$ (solid lines) on the Debye functions with different R_g for SANS from the mixture SI/DS 30/70. σ_P = 5.00, 4.42, and 4.18 nm was obtained for R_g = 7, 6, and 3 nm (dashed lines), respectively.

which is in the same order as the radius of gyration for both DS and PS block chains.

It should be noted that the estimated value of t_P may have an error originating from the error in subtracting $I_t(q)$ as discussed in section IV.4. To reduce the error for the evaluation of t_P as much as possible, we try to weight the portion of the profiles $I_d(q)$ in the q range 0.1 nm^{-1} < $q \leq q_c$, where q_c is defined in Figure 13 and the lower limit of q (0.1 nm^{-1}) is determined from curve b in Figure 15: this limit corresponds to the one above which $I_{total}(q)$ is predicted to show the asymptotic behavior given by eq 12. The value $t_P \cong 12.5$ nm was obtained when the subtraction of $I_t(q)$ (eqs 5 and 6) was conducted by using R_g = 7 nm in eq 8 (see curve 2 in Figure 8). Changing the value R_g to 6 and 3 nm gave rise to t_P = 11.1 and 10.5 nm, respectively (see curves 3 and 4 in Figure 8). This curve-fitting procedure for the mixtures 30/70 using Debye functions with R_g = 7, 6, and 3 nm (dashed lines) is shown in Figure 18 along with the best-fit $I_d(q)$ (solid lines) with σ_P = 5.00, 4.42, and 4.18 nm (t_P = 12.5, 11.1, and 10.5 nm), respectively. Thus, estimation of t_P is fairly insensitive to the value of R_g, and the depth of interpenetration between DS and PS brush is evaluated to be 11 ± 1 nm.

This characteristic interface thickness between DS and PS was compared with the value predicted by the theory of Shull et al.[5,28] developed for diblock copolymer/homopolymer mixtures in the strong segregation regime. In the case of r_S > 1, t_P is approximated by the equation

$$t_P \cong 1.09R_{gPS} + 3.16[(R_{gPS})^2/(1 - \Phi_h)D_{PS}] \quad (13)$$

where Φ_h is the volume fraction of homopolystyrene in the domain composed of the PS block chains and homopolystyrene chains, R_{gPS} is the unperturbed radius of gyration of the PS block chain, and D_{PS} the thickness of the polystyrene microdomain comprising the PS block chains and DS. For the SI/DS mixture with 30/70 composition $D_{PS} = \bar{D} - D_{PI} = D_0/(1 - \Phi_{DS}) - D_{PI}$ = 171 nm (D_0 = 61.0 nm, D_{PI} = 30.4 nm, and Φ_h = 0.182) and R_{gPS} = 7.0 nm. Then t_P is estimated to be 12.8 nm. This value is consistent with 11 ± 1 nm evaluated from the SANS analysis.

In the limiting case of small Φ_{DS} in which ΔB_1 is sufficiently small due to the overlap of the opposing PS brushes, the contribution of the second term of eq 12 having ΔB_2 and σ_I becomes dominant to the scattering function. Thus, the scattering profile is expected to be "SAXS-like", i.e., having approximately the q^{-4} behavior. The fact that the mixtures of SI/DS with 80/20 and 70/30 compositions show the asymptotic behavior of q^{-4} may support this, though this conclusion is contradictory to our rough estimation that the PS brushes tend to overlap at Φ_{DS} smaller than ca. 0.16, the derivation of which will be mentioned in Appendix II. In Figure 17 the solid lines fit to the scattering profiles for 80/20 and 70/30 were obtained under the following requirements: (i) ΔB_1 is equal to the average of the scattering lengths of PS and DS weighted by their volume fractions in the PS phase and (ii) σ_I in eq 12 is equal to that estimated by SAXS. The SAXS-like asymptotic behaviors for 80/20 and 70/30 are well reproduced, but more detailed discussion based on the exact spatial distribution of DS will be a future work.

The underestimation of the critical concentration for the overlap of the PS brushes $\Phi_{overlap}$ may be due to the underestimation of the interface thickness between the PS block chains and DS. We employed the characteristic interface thickness t_P to evaluate the limit of the extension of the PS block chains. However, the actual interface has much longer tail into the DS region, as

represented by the error function, and the scattering profiles are affected as well. Therefore, $\Phi_{overlap}$ estimated from the SAXS-like asymptotic behaviors of 80/20 and 70/30 may be 0.3.

V. Conclusion

Self-assembly of the binary mixtures of lamella-forming block copolymer SI and homopolymer HS (or DS) in the solution-cast and subsequently annealed films was investigated as a function of homopolymer content Φ_{HS} (or Φ_{DS}) under the particular condition $r_S \cong 1$, where the PS block chains behave as a dry brush. The combination of SAXS, SANS, and TEM techniques was found to be crucial to elucidate the self-assembly for such a complicated system. SAXS and TEM, both of which have a contrast between the PS and PI phases, elucidated that, regardless of homopolymer content, the PI microdomains maintain the lamellar shape with a uniform thickness in the matrix composed of PS block chains and HS (or DS), although an increase of the homopolymer content increases the interlamellar distance $\bar{D}$, its distribution σ_D, and the interface thickness between the PS and PI phases t_I. The TEM observation is especially superior in the investigation of the undulation of the lamellar sheets and the vesicular morphologies made by them and in directly providing the nonexistence of the macrophase separation. On the other hand, the SAXS technique is superior for investigating the spatial arrangements of the PI lamellae (σ_D and $\bar{D}$), their thickness (D_{PI}) and thickness distribution (σ_{PI}), and the interface thickness $t_{I,SAXS}$. SANS with the deuterium labeling technique elucidated that the penetration depth of DS into the PS brush t_P is 11 ± 1 nm for the SI/DS mixtures. The determination of t_P was made possible by utilizing the pieces of information obtained by SAXS such as $\bar{D}$, D_{PI}, and $t_{I,SAXS}$. This penetration depth is comparable to the unperturbed radius of gyration of DS, consistent with a theoretical prediction[5,28] and with the dry brush picture in the spatial distribution of DS.

Acknowledgment. We are grateful to Kuraray Co., Ltd., for supplying H102 and Tosoh Co., Ltd., for S62. This work was supported in part by a Grant-in-Aid for Scientific Research (05650673) from the Ministry of Education, Science and Culture, Japan.

Appendix I

Here we summarize the scattering formula for the one-dimensional paracrystal model with a perferred orientation. The polyisoprene lamellae are represented by disks A with an average disk thickness D_A and a radius R. The disks are stacked with their normals along the z_1-axis as shown in Figure 8a. We assume that the radius of a disk R is monodisperse in size, while the disk thickness has polydispersity in size. The scattering intensity for one-dimensional assembly of the disks along the z_1-axis is given by

$$I(q) = C\sum_{j,k}^{N}\langle f_j f_k^* \exp(iq_z z_{jk})\rangle \quad \text{(A-1)}$$

$$C = 4V^2A_e^2\Delta\varrho^2[J_1(\omega)/\omega]^2, \qquad \omega = R(q_x^2 + q_y^2)^{1/2} \quad \text{(A-2)}$$

where q_z is the scattering vector parallel to the z_1-axis and q_x and q_y are the scattering vector normal to the z_1-axis. z_{jk} is the distance between the jth and kth disks along the z_1-axis, and N is the number of the disks in the stack. The symbol $\langle\ \rangle$ denotes the ensemble average, i.e., the average of the scattering intensity for many assemblies. The proportionality constant C is given by the Bessel function of the first kind of first-order J_1, which is a function of the lateral dimension of the disks R, the volume of the disks V, the scattering amplitude from an electron A_e, and the excess electron density of the disks with respect to the medium $\Delta\varrho$. f_j is the scattering amplitude of the jth disk having the disk thickness D_j and the characteristic interface thickness $t_I = (2\pi)^{1/2}\sigma_I$

$$f_j = \sin(q_z D_j/2)/(q_z D_j/2)\exp(-\sigma_I^2 q_z^2/2) \quad \text{(A-3)}$$

Hosemann's one-dimensional paracrystal model[19] is employed to express the distance statistics $H(z)$

$$H(z) = (2\pi\sigma_D^2)^{-1/2}\exp[-(z-\bar{D})^2/2\sigma_D^2] \quad \text{(A-4)}$$

where $\bar{D}$ and σ_D are the average and the standard deviation of the interdomain distance D, respectively. The scattering intensity $I(q:\alpha,\Omega)$ from a single grain (a single assembly of the disks) oriented at (α,Ω) with respect to the laboratory-fixed coordinate shown in Figure 8a is given by

$$I(q:\alpha,\Omega) = 4NV^2A_e^2\Delta\varrho^2[J_1(\omega)/\omega]^2 I_1(q_z:\alpha,\Omega) \quad \text{(A-5)}$$

$$I_1(q_z:\alpha,\Omega) = [\langle|f^2|\rangle - |\langle f\rangle|^2] + |\langle f\rangle|^2[Z + I_c/N] \quad \text{(A-6)}$$

The term I_c is the zero-order scattering intensity which is important only at very small q near $q \cong 0$ under the condition that N is less than 10. Z is the lattice factor given by

$$Z = (1 - |F|^2)/(1 - 2|F|\cos(q_z\bar{D}) + |F|^2) \quad \text{(A-7)}$$

and F is given by the Fourier transformation of the distance statistics, $H(z)$

$$F(q_z) = \int H(z)\exp(-iq_z z)dz = |F(q_z)|\exp(-iq_z\bar{D}) \quad \text{(A-8)}$$

with

$$|F(q_z)| = \exp(-\sigma_D^2 q_z^2/2) = \exp(-g^2\bar{D}^2 q_z^2/2) \quad \text{(A-9)}$$

The quantity g is Hosemann's g parameter defined as $g \equiv \sigma_D/\bar{D}$.

For the preferentially oriented system, $I(q:\alpha,\Omega)$ should be averaged with the orientation distribution $w(\alpha,\Omega)$ of the assemblies. This averaged scattered intensity along the z-axis is given by[20]

$$I(q) \equiv \int_0^{\pi}\int_0^{2\pi} I(q:\alpha,\Omega)w(\alpha,\Omega)\sin\alpha d\alpha d\Omega \Big/ \int_0^{\pi}\int_0^{2\pi} w(\alpha,\Omega)\sin\alpha d\alpha d\Omega$$
$$\sim NV^2A_e^2\Delta\varrho^2 q^{-2} I_1(q) \quad \text{(A-10)}$$

where $I_1(q)$ is the scattering intensity distribution for the one-dimensional assembly along its axis, i.e., z_1-axis, for the assembly shown in Figure 8a, and q is magnitude of the scattering vector along this axis. $I_1(q)$ is given by eq A-6, where q_z should be replaced by q. Equation A-10 is valid for the special case satisfying the following criteria: (i) The lateral size of disk R is much larger

than its distance $\bar{D}$ so that the scattering from the assembly shown in Figure 8a is nonzero only along the z_1-axis and the scattering perpendicular to the z-axis decays with $q = (q_x^2 + q_y^2)^{1/2}$ according to the delta function, in the q range of our interest, i.e., $q \geq 1/\bar{D}$. (ii) All assemblies having different orientation (α,Ω) are identical. Our systems satisfy these criteria. The factor q^{-2} in eq A-10 is called the Lorentz factor.

As the distribution in the interdomain distance increases, the lattice factor Z in eq A-7 approaches unity. In this limit the interdomain interference is not important, i.e., $I_1(q_z;\alpha,\Omega) = \langle|\langle f\rangle|^2\rangle$. Therefore, the scattering intensity can be described by the scattering from the isolated PI lamellae of thickness D_{PI} with a certain orientation distribution in 3D space and is given by

$$I(q;D_{PI}) \sim \Delta\varrho^2(AD_{PI})^2q^{-2}\sin^2(qD_{PI}/2)/(qD_{PI}/2)^2 \quad \text{(A-11)}$$

Here A is the flat area of the interface of PI lamellae; $A \sim \zeta^2$, where ζ is the persistence length of the interface.

Appendix II

Here we estimate the critical concentration of DS $\Phi_{overlap}$ below which the opposing PS brushes start to overlap in the SI/DS mixtures, assuming that the characteristic interface thickness t_P between PS and DS estimated for the mixtures having large Φ_{DS} (as shown in Figure 16a–c) is valid even for the mixtures having smaller Φ_{DS} in the criterion satisfying $\Phi_{DS} \geq \Phi_{overlap}$ (as shown in Figure 16d,e). For simplicity the profile of the interface between the PS brush and DS is represented by the triangle with the thickness t_P instead of the error function type. Then insertion of the DS phase with thickness t_P into the center of the PS microdomain as illustrated in Figure 16d,e just starts to separate the opposing PS brushes from each other. This concentration of DS corresponds to $\Phi_{overlap}$, and the ratio of the volumes occupied by the DS homopolymer and the PS block chains gives the relation

$$\Phi_{overlap}/[(1 - \Phi_{overlap})/2] = t_P/(D_0 - D_{PI}) \quad \text{(A-12)}$$

because PS and PI block chains occupy half of the volume of the SI microdomains. Substituting $D_0 = 61$ nm, $D_{PI} = 32$ nm, and $t_P = 11$ nm, one gets $\Phi_{overlap} = 0.16$.

References and Notes

(1) Berney, C. V.; Cheng, P.; Cohen, R. E. *Macromolecules* **1988**, *21*, 2235.
(2) Hashimoto, T.; Tanaka, H.; Hasegawa, H. *Macromolecules* **1990**, *23*, 4378.
(3) Winey, K. I.; Thomas, E. L.; Fetters, L. J. *Macromolecules* **1991**, *24*, 6182.
(4) Koizumi, S.; Hasegawa, H.; Hashimoto, T. *Makromol. Chem., Makromol. Symp.* **1992**, *62*, 75.
(5) Shull, K. R.; Mayes, A. M.; Russell, T. P. *Macromolecules* **1993**, *26*, 3929.
(6) Tanaka, H.; Hasegawa, H.; Hashimoto, T. *Macromolecules* **1991**, *24*, 240.
(7) Winey, K. I.; Thomas, E. L.; Fetters, L. J. *Macromolecules* **1992**, *25*, 2645.
(8) Leibler, L.; Pincus, P. A. *Macromolecules* **1984**, *17*, 2922.
(9) Whitmore, M. D.; Noolandi, J. *Macromolecules* **1985**, *18*, 657.
(10) Roe, R.-J. *Macromolecules* **1986**, *19*, 728.
(11) Kinning, D. J.; Thomas, E. L.; Fetters, L. J. *J. Chem. Phys.* **1989**, *90*, 5806.
(12) Kinning, D. J.; Winey, K. I.; Thomas, E. L. *Macromolecules* **1988**, *21*, 3502.
(13) Koizumi, S.; Hasegawa, H.; Hashimoto, T. *Macromolecules* **1994**, *27*, 6532.
(14) Mayes, A. M.; Russell, T. P.; Satija, S. K.; Majkrzak, C. F. *Macromolecules* **1992**, *25*, 6523.
(15) Hyde, S. T.; Fogden, A.; Ninham, B. W. *Macromolecules* **1993**, *26*, 6782.
(16) Hasegawa, H.; Hashimoto, T.; Hyde, S. T. Unpublished results.
(17) Katano, S.; Suzuki, J.; Koizumi, S. Unpublished results.
(18) Porod, G. *Kolloid-Z., Z. Polym.* **1951**, *124*, 83; **1952a**, *125*, 51; **1952b**, *125*, 108.
(19) Hosemann, R.; Baguchi, S. N. *Direct Analysis of Diffraction by Matter*; North-Holland: Amsterdam, The Netherlands, 1962.
(20) Shibayama, M.; Hashimoto, T. *Macromolecules* **1986**, *19*, 740.
(21) Hashimoto, T.; Todo, A.; Itoi, H.; Kawai, H. *Macromolecules* **1977**, *10*, 377.
(22) Hashimoto, T.; Shibayama, M.; Kawai, H. *Macromolecules* **1980**, *13*, 1237.
(23) Hendricks, R. W. *J. Appl. Crystallogr.* **1972**, *5*, 302.
(24) Ruland, W. *J. Appl. Crystallogr.* **1971**, *4*, 70.
(25) Hashimoto, T.; Kawamura, T.; Harada, M.; Tanaka, H. *Macromolecules* **1994**, *27*, 3063.
(26) Jinnai, H.; Hasegawa, H.; Hashimoto, T.; Han, C. C. *Macromolecules* **1991**, *24*, 282.
(27) de Gennes, P. G. *Scaling Concepts in Polymer Physics*; Cornell University Press: Ithaca, NY, 1979.
(28) Shull, K. R.; Winey, K. I. *Macromolecules* **1992**, *25*, 2637.